Archives of Biochemistry and Biophysics 752 (2024) 109859

Contents lists available at ScienceDirect

Archives of Biochemistry and Biophysics

journal homepage: www.elsevier.com/locate/yabbi

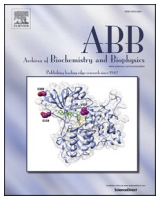

Brief communication

Ligand bound structure of a 6-hydroxynicotinic acid 3-monooxygenase provides mechanistic insights

Zachary R. Turlington [a], Sofia Vaz Ferreira de Macedo [a], Kay Perry [b], Sam L. Belsky [c], Jennifer A. Faust [c], Mark J. Snider [c], Katherine A. Hicks [a,*]

[a] Department of Chemistry, State University of New York at Cortland, Cortland, NY, 13045, United States
[b] NE-CAT and Department of Chemistry and Chemical Biology, Cornell University, Argonne National Laboratory, Argonne, IL, United States
[c] Department of Chemistry, The College of Wooster, Wooster, OH, 44691, United States

ARTICLE INFO

Keywords:
Flavin monooxygenase
Bacterial nicotinic acid metabolism
Flavin adenine dinucleotide (FAD)
Protein structure

ABSTRACT

6-Hydroxynicotinic acid 3-monooxygenase (NicC) is a bacterial enzyme involved in the degradation of nicotinic acid. This enzyme is a Class A flavin-dependent monooxygenase that catalyzes a unique decarboxylative hydroxylation. The unliganded structure of this enzyme has previously been reported and studied using steady- and transient-state kinetics to support a comprehensive kinetic mechanism. Here we report the crystal structure of the H47Q NicC variant in both a ligand-bound (solved to 2.17 Å resolution) and unliganded (1.51 Å resolution) form. Interestingly, in the liganded form, H47Q NicC is bound to 2-mercaptopyridine (2-MP), a contaminant present in the commercial stock of 6-mercaptopyridine-3-carboxylic acid(6-MNA), a substrate analogue. 2-MP binds weakly to H47Q NicC and is not a substrate for the enzyme. Based on kinetic and thermodynamic characterization, we have fortuitously captured a catalytically inactive H47Q NicC•2-MP complex in our crystal structure. This complex reveals interesting mechanistic details about the reaction catalyzed by 6-hydroxynicotinic acid 3-monooxygenase.

1. Introduction

N-Heterocyclic aromatic compounds (*N*HACs) are common to many pharmaceuticals, herbicides and pesticides and are a focus for bioremediation [1–3]. *N*HACs have been found to be environmentally harmful due to their high-water solubility and their mutagenic, carcinogenic, and toxic characteristics [4–8]. A bacterial degradation pathway has been identified in the harmless, soil-dwelling bacteria *Pseudomonas putida* that breaks down the model *N*HAC, nicotinic acid (NA), into a less harmful compound, fumarate [9]. As shown in Scheme 1, the focus of this study is 6-hydroxynicotinate 3- monooxygenase (NicC; E.C. 1.14.13.114), whose biological role is to catalyze the conversion of 6-hydroxynicotinic acid (6-HNA) to 2,6-dihydroxypyridine (2,6-DHP) via a decarboxylative hydroxylation mechanism [10,11].

Wild-type *P. putida* NicC has been previously structurally characterized and belongs to the Class A flavin dependent monooxygenase superfamily [10]. These enzymes use the cofactors nicotinamide adenine dinucleotide or nicotinamide adenine dinucleotide phosphate (NADH or NADPH) and flavin adenine dinucleotide (FAD) during catalysis [12,13]. Attempts to further understand the structural basis for 6-HNA (substrate) binding by crystallizing and determining a substrate-bound structure of the wild-type enzyme have previously been unsuccessful. However, we have reported a potential substrate (6-HNA) bound state using computational modeling [10].

To further explore the structural determinants of substrate (6-HNA) binding we characterized the effects of replacing active site residues with alanine or more conservative residues. Based on the resulting kinetic analysis of *Bordetella bronchiseptica* NicC, His47 was determined to be a critical active site residue [10,11]. Although the H47A NicC variant resulted in an enzyme unable to bind FAD, the H47E variant retained some ability to bind FAD. UV-titration of the H47E variant with 6-HNA revealed that this alteration lowered the enzyme's affinity for 6-HNA by more than 350-fold, and reduced the turnover of the substrate hydroxylation (and decarboxylation) to 0.02% of the wild type enzyme [11]. These functional consequences and further structural analyses of the *Pseudomonas putida* NicC homologue [10] led us to hypothesize that His47 is important, along with Tyr215, in stabilizing the ionized form of 6-HNA at the active site. The *B. bronchiseptica* and *P. putida* NicC enzymes are homologues that are 61% identical and 77% similar in

* Corresponding author.
E-mail address: katherine.hicks@cortland.edu (K.A. Hicks).

https://doi.org/10.1016/j.abb.2023.109859
Received 31 October 2023; Received in revised form 8 December 2023; Accepted 11 December 2023
Available online 16 December 2023

Abbreviations

6-MNA	6-mercaptopyridine-3-carboxylic acid
2-M-5-P	2-mercapto-5-hydroxypyridine
2-MP	2-mercaptopyridine
6-HNA	6-hydroxynicotinic acid
2,5-DHP	2,5-dihydroxypyridine
*N*HACs	*N*-heterocyclic aromatic compounds
NA	nicotinic acid
FAD	flavin adenine dinucleotide
PCR	polymerase chain reaction
NCS	Non-crystallographic symmetry
NADH	nicotinamide adenine dinucleotide (reduced form)
PHBH	*p*-hydroxybenzoate hydroxylase
MHPCO	2-methyl-3-hydroxypyridine-5-carboxylic acid oxygenase

primary sequence [10]. Since the H47E introduced extra negative charge in the active site, we decided to characterize the effects of a *P. putida* H47Q NicC variant. Due to the neutral polar nature of glutamine and its relatively small size, we hypothesized that a H47Q variant may accommodate a greater variety of substrates. We therefore shifted our structural studies from the wild-type enzyme to the *P. putida* H47Q NicC variant.

In this work, we engineered and purified the H47Q NicC variant from *P. putida* as this homologue is more amenable to crystallization due to the presence of an *N*-terminal transmembrane helix on *B. bronchiseptica* NicC. We observed that the *P. putida* H47Q variant had high FAD occupancy. Diffraction data were collected on a single crystal of H47Q NicC to determine the structure of the unliganded form. We then attempted to cocrystallize the H47Q NicC with a 6-HNA analogue, 6-mercaptopyridine-3-carboxylic acid (6-MNA), to obtain anomalous sulfur difference density to aid in ligand placement [14,15]. This data collection strategy would ensure that any observed electron density at the putative active site was due to the presence of the ligand. Interestingly, the cocrystallized variant revealed the structure of an enzyme•2-mercaptopyridine (2-MP) complex. Mass spectrometric analysis revealed that 2-MP is a contaminant present in the commercial stock of 6-MNA. While 2-MP binds weakly to H47Q NicC, it is not a substrate for the enzyme. Therefore, after binding to the active site, 2-MP remained in the active site allowing us to capture the E•2-MP complex using protein X-ray crystallography. Comparison of the H47Q NicC unliganded and liganded structures reveals the identity of active site residues important for substrate binding and catalysis.

2. Materials and methods

Site-directed mutagenesis. The molecular cloning of the *nicC* gene from *P. putida* KT2440 has been previously described [10]. The polymerase chain reaction (PCR)-based engineering of the H47Q variant of NicC was done using the Q5 Site-Directed Mutagenesis Kit (New England Biolabs, Ipswich, MA). The entire gene was sequenced to confirm the successful creation of each nucleotide substitution. The sequence of the primers used to generate the mutation are shown in Table S1.

Enzyme expression and purification. Variant H47Q PpNicC was overproduced in BL21 (DE3) cells (Novagen) and purified using both nickel ion affinity and gel filtration chromatography, as previously described [10,11]. Protein purity was confirmed by sodium dodecyl sulfate−polyacrylamide gel electrophoresis analysis. For crystallization trials, a cryoprotectant was not included in the storage buffer. Instead, purified protein was exchanged into storage buffer [50 mM Tris pH 7.5, 150 mM NaCl and 1 mM DTT] using a 10DG column (Bio-Rad), concentrated to approximately 6 mg/mL, flash-frozen in liquid nitrogen, and stored as aliquots at −80 °C.

Crystallization and Data Collection. Initial crystallization conditions for the H47Q PpNicC variant were identified using Crystal Screens 1 and 2, and Index Screen (Hampton Research). Crystallization trials were done using the hanging drop vapor diffusion method and drops were formed by mixing 1.5 μL of reservoir solution with 1.5 μL of protein sample at 18 °C. In 5 days, initial microcrystals were harvested and crushed for seeding using seed bead (Hampton Research). With seeding, diffraction-quality crystals grew in 4–5 days that were diffraction quality in 0.1 M Hepes, pH 7.5, 15–25% polyethylene glycol (PEG) 3350, and 0.2 M magnesium chloride hexahydrate.

For the liganded crystals, 1 mM 6-MNA was incubated with the protein solution for 1 h prior to tray set-up. The crystallization solution was as described above. The 6-MNA stock was purchased at the highest possible purity, approximately 90%, from Sigma Aldrich. Bright yellow, rod-shaped crystals grew in 4–5 days that were approximately 100–150 μm × 20–30 μm. For cryoprotection, the crystallization buffer was supplemented with 15% 1,2 propanediol (unliganded) or 10% ethylene glycol (liganded). After incubation in the cryoprotecting buffer, the samples were flash frozen in liquid nitrogen.

Diffraction data for the liganded and unliganded H47Q NicC were collected at NEC-CAT beamline 24-ID-C. For the unliganded structure, data were collected at wavelength 0.98 Å with 0.2° oscillations. For the liganded structure, data were collected at a wavelength of 1.77 Å with 0.2° oscillations to calculate sulfur difference density. The data were automatically indexed and reduced by RAPD (https://github.com/RAPD/RAPD), the data-processing pipeline implemented at NE-CAT.

Structure Determination, Model Building, and Refinement. The H47Q NicC structure was determined using the molecular replacement pipeline on RAPD. For the liganded structure, an anomalous difference Fourier was calculated to show the anomalous peaks for sulfur atoms using the fast Fourier transform program in the CCP4 suite [16]. Refinement was carried out using PHENIX [17] and iterative rounds of manual model building were done using COOT [16,18]. Non-crystallographic symmetry (NCS) was not detected so it was not part of the refinement strategy. During the later rounds of refinement, water, FAD, and 2-MP molecules were added to the model. Geometry

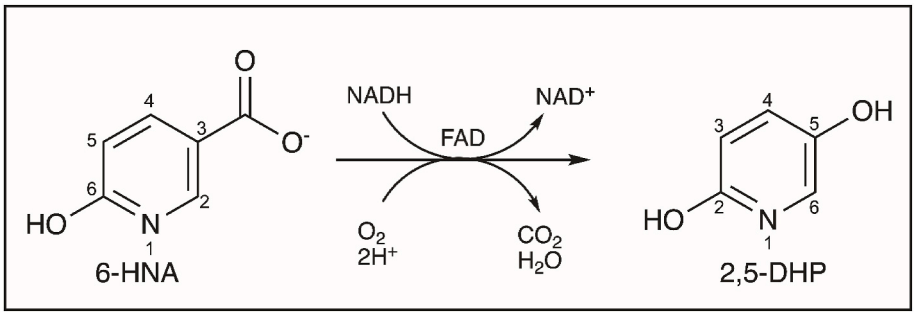

Scheme 1. NicC is a flavin-dependent monooxygenase that catalyzes the conversion of 6-hydroxynicotinate (6-HNA) to 2,5-dihydroxypyridine (2,5-DHP).

was verified by MolProbity [19]. Data collection and refinement statistics are summarized in Table S2. The liganded H47Q PpNicC structure has the PDB ID 8UIQ and the unliganded H47Q PpNicC structure has the PDB ID 8UIV.

Equilibrium Binding. Separate solutions of WT NicC and the H47Q variant of NicC (1.0 mL; 30 μM) in sodium phosphate buffer (50 mM, pH 7.5) were titrated by stepwise addition of a solution of 6-MNA, 6-HNA, or 2-MP in the same buffer at 25 °C. The changes in absorbance at 450 nm (A450) were measured using a dual beam spectrophotometer after allowing the solution to equilibrate for 1 min. The absorbance values were corrected for dilution and baseline corrected by subtracting the absorbance at 700 nm. The ΔA450 signal in the 6-MNA titration was also corrected to remove the absorbance at 450 nm from 6-MNA. The ΔA450 was fit by nonlinear regression to the hyperbolic binding equation (Eq (1)) using KinTek Explorer (v1) to determine the K_d of each E_{ox}·ligand (L) complex:

$$\Delta A(450) = \frac{a[L]}{K_d + [L]} \quad \text{(eq 1)}$$

Steady-State Kinetic Analyses. First, a reaction containing the H47Q NicC variant (1 μM), NADH (100 μM) and 6-HNA (1 mM) in sodium phosphate buffer (50 mM, pH 7.5) was monitored spectrophotometrically at 340 nm until the reaction reached equilibrium (10 min). Accounting for the molar absorbance coefficients of NAD^+ and 2,5-dihydroxypyridine at 340 nm the stoichiometry of the reaction was determined to be more highly coupled (98.5%) than that of the reaction catalyzed by WT NicC (90%) [20]. Due to the tight coupling, reaction rates measured by following NADH oxidation report on the overall reaction. Steady-state kinetic analysis of the *P. putida* H47Q NicC variant was measured using the method of initial rates at 340 nm ($\Delta\varepsilon_{340nm}$ = 6220 $M^{-1}cm^{-1}$) or 370 nm ($\Delta\varepsilon_{370nm}$ = 2626 $M^{-1}cm^{-1}$). Assays contained 50 nM enzyme and either a constant concentration of NADH (150 μM) with a series of 6-HNA concentrations (12.5–1000 μM), or with constant concentration of 6-HNA (20 μM) and a series of NADH concentrations (25–300 μM). All initial rates were replicated at least once and fit with the Michaelis Menten equation modified to include uncompetitive inhibition by 6-HNA (Eq (2)).

$$v = \frac{V_m[S]}{[S] + K_M + [S]^2/K_i} \quad \text{(eq 2)}$$

HPLC kinetic analysis. Solutions of NADH (100 μM), 2-MP (250 μM), NicC (350 nM wild-type or H47Q) in 50 mM sodium phosphate buffer, pH 7.5 were incubated at 25 °C for 1.5 h. The enzyme was then removed from the reaction mixture using a centrifugal filter and the small molecule products were analyzed by HPLC. The aqueous phase consisted of 20 mM ammonium acetate, pH 7.0 and the organic phase was 100% methanol. A shallow gradient from 1% to 1.6% methanol was run over 10 min on a Phenomenex Luna Omega 3 μm Polar C18 column. The elution profiles were then analyzed at 340 nm.

LC-MS analysis. Solutions of 6-MNA (1 mM) in sodium phosphate buffer (50 mM, pH 7.5) were incubated with NADH (1 mM) and enzyme (0.5 μM; WT or H47Q) for 1 h. Control reactions were also performed in the absence of NADH and enzyme. After removing the enzyme from solution by ultrafiltration (Amicon centrifugal filter; 10,000 MWCO), aliquots (5 μL) of the resulting product solutions were separated and analyzed using an Agilent 1200 Series HPLC with Agilent 6410 triple quadrupole mass spectrometer. Chromatography utilized a Luna Omega 3 μm Polar C18 (100 × 2.1 mm) column with a mobile phase of 5 mM ammonium acetate in water (A) and 5 mM ammonium acetate in 95% methanol (B) with a gradient of 1% B to 2% B over 10 min at a flow rate of 0.25 mL/min. The mass spectra were collected using electrospray ionization in negative mode with a fragmentor voltage of 135 V for MS2 scans.

Figure preparation. Figures were generated using the PyMOL molecular graphics system, version 2.5, (Schrödinger, LLC), ChemDraw (CambridgeSoft), and KaleidaGraph, version 5.0 for Mac (Synergy Software).

3. Results and discussion

H47Q variant is catalytically active. Substitution of His47 with glutamine results in a kinetically active *P. putida* NicC variant. Intriguingly, this variant demonstrates substrate inhibition (uncompetitive) when varying 6-HNA concentration and standard saturation kinetics with NADH (Fig. 1A). In a previously reported study [20], two 6-HNA binding sites were necessary to model the observed mechanism of 6-HNA binding by wild type *B. bronchiseptica* NicC. The binding of 6-HNA in this second site apparently causes weak uncompetitive inhibition, with a 6-HNA K_i = 20 ± 4 mM [20]. The kinetic analysis of the *P. putida* H47Q variant here indicates that this active site substitution causes a significant decrease in both the 6-HNA K_M (2 μM (H47Q) vs 97 μM (wild-type)) and the 6-HNA K_i (0.28 ± 0.07 mM, H47Q). Thus, the observed inhibition by the 6-HNA substrate is more pronounced in the H47Q variant. In contrast, the $V_{max}/[E]$ is only slightly slower for H47Q (0.86 ± 0.08 s^{-1}) compared to wild type NicC (2.2 s^{-1}) [10]. Previously measured kinetic constants for *P. putida* and *B. bronchiseptica* NicC wild type and variant enzymes are provided in Table S3 [10,11,20].

Prior kinetic analysis of the *Bordetella* H47E NicC variant resulted in an enzyme that could bind to FAD, but had catalytic activity too low to measure using the continuous spectrophotometric assay that measures NADH oxidation [11]. Using an HPLC-based assay to quantify and compare the concentrations of the NAD^+ and 2,5-DHP products, the catalytic cycles of both the Y215F and H47E *B. bronchiseptica* NicC variants were observed to show an uncoupling of the oxidation and hydroxylation (*i.e.* $[NAD^+] \gg [2,5\text{-DHP}]$), and exhibited significantly reduced rates of 2,5-DHP formation. Based on these data and the kinetic data on the *P. putida* H47Q NicC variant (Fig. 1A), His47 and Tyr215 are important active site residues involved in stabilizing the ionized form of 6-HNA necessary for electrophilic aromatic substitution [11,20].

Measurement of the steady-state kinetic parameters with the 6-MNA substrate analogue is not possible using the standard UV–visible absorbance based assay that monitors NADH oxidation at 340 or 370 nm [10,11] as 6-MNA absorbs strongly at these wavelengths (Fig. S1). Therefore, the catalytic activity of the H47Q NicC variant with 6-MNA was measured by incubating the enzyme and substrate and analyzing the resulting product(s) using LC-MS. As shown in Figs. S2 and S3, the LC-MS data indicate that the resulting product of the H47Q NicC-catalyzed reaction has an *m/z* ion that corresponds to that of the expected enzymatic product, 2-mercapto-5-hydroxypyridine (2-M-5-P). There is also evidence of possible product dimer formation due to disulfide bond formation.

6-MNA binds weakly to NicC. The dissociation constant of the E·6-MNA complex was determined by measuring the perturbation in the bound flavin absorbance at 450 nm upon binding 6-MNA (Fig. 1B). The equilibrium titration data reveal that the 6-MNA substrate analogue binds with a ~3-fold lower affinity to the H47Q variant than the natural 6-HNA substrate (K_d of 2.9 ± 0.1 mM as compared to 1.1 ± 0.1 mM, respectively; Fig. 1B). The wild-type enzyme's affinity for 6-MNA (K_d = 2.7 ± 0.1 mM; Fig. S4) is similar to that of the H47Q variant with 6-MNA, whereas, in comparison, wild-type NicC has been observed to bind 6-HNA 27× more tightly than 6-MNA [11]. This lower binding affinity for between H47Q NicC and 6-MNA aids in explaining the low occupancy observed for the ligand in the active site, as discussed below.

Comparison of the wild-type and variant NicC structures. As shown in Fig. S5A, the overall structure of unliganded H47Q NicC and wild-type NicC (PDB ID: 5EOW) are nearly identical indicating that the active site mutation did not affect the overall protein structure. A comparison of the overall structure of the H47Q variant in the presence and absence of ligand is shown in Fig. S5B. As shown by superposition of the structures, there are no major changes in the overall structure of the H47Q NicC variant upon ligand binding. Studies primarily done on *p*-

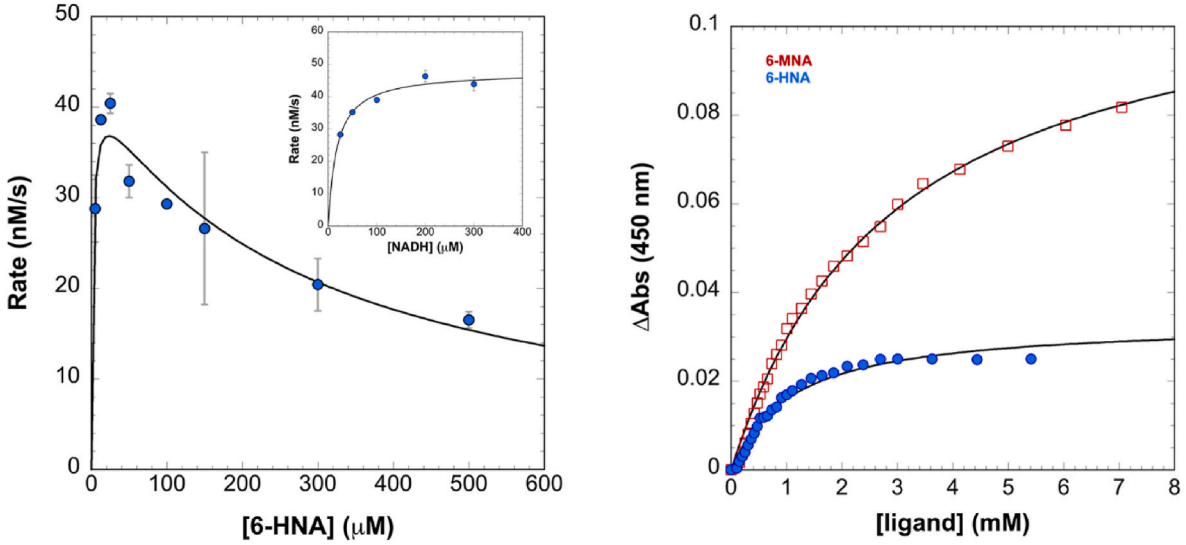

Fig. 1. Catalytic activity of NicC with 6-HNA and the binding of 6-MNA. **A.** Steady-state kinetic analysis of NicC variant H47Q with 6-HNA indicate substrate inhibition. Data fits to $V_{max}/[E] = 0.86 \pm 0.08\ s^{-1}$, K_M (6-HNA) $= 2 \pm 1$ μM, and K_i (6-HNA) $= 0.28 \pm 0.07$ mM. Inset shows initial rates measured with constant concentrations of 6-HNA of 20 μM ($10 \times K_M$) and enzyme (50 nM) with increasing concentrations of NADH (25–300 μM). Data fit with the Michaelis-Menten equation estimate a K_M (NADH) of 18 ± 3 μM and $V_{max}/[E] = 0.95 \pm 0.03\ s^{-1}$ **B.** Equilibrium titrations of the H47Q variant of NicC (30 μM) with 6-HNA (blue circles) and 6-MNA (red squares) fit to the hyperbolic binding equation estimates a K_d for E·6-MNA of 2.9 ± 0.1 mM and K_d for E·6-HNA of 1.1 ± 0.1 mM.

hydroxybenzoate hydroxylase (PHBH) has shown that the isoalloxazine ring of FAD changes conformations during catalysis from an "out" [21] to an "in" [22] to an "open" [23] conformation. Our previous work has indicated that Tyr215 and His47 play a decisive role in triggering flavin movement from the "in" to "out" position upon forming a reactive E•S complex [11,20]. As shown in Fig. S5B, in both the liganded and unliganded H47Q NicC structure the FAD isoalloxazine ring is in the "in" conformation, which is also its conformation in the previously determined wild-type structure [10]. This is the catalytically active FAD conformation in which the substrate is hydroxylated by the flavin hydroperoxide [22].

The H47Q NicC active site contains 2-mercaptopyridine (2-MP). When H47Q was co-crystallized with the native 6-HNA substrate there was no electron density seen in the active site that could be clearly assigned as ligand density. However, we often did observe the presence of electron density likely corresponding to disordered water or ligand molecule(s) (data not shown). In the electron density resulting from the H47Q variant co-crystallized with 6-MNA, planar electron density was observed in the active site suggesting that this density was not due to an ion or water molecule, which would have more rounded/spherical density. By examining the sulfur difference density, we could determine that the molecule bound in the active site had a sulfur atom. However, there was no evidence of the carboxylate group on the ligand or hydroxyl, as would be expected if there was product formation (Fig. S3). As shown in Fig. S6, we interpret the weak electron density near the FAD isoalloxazine ring as 2-mercaptopyridine (2-MP) and have modeled 2-

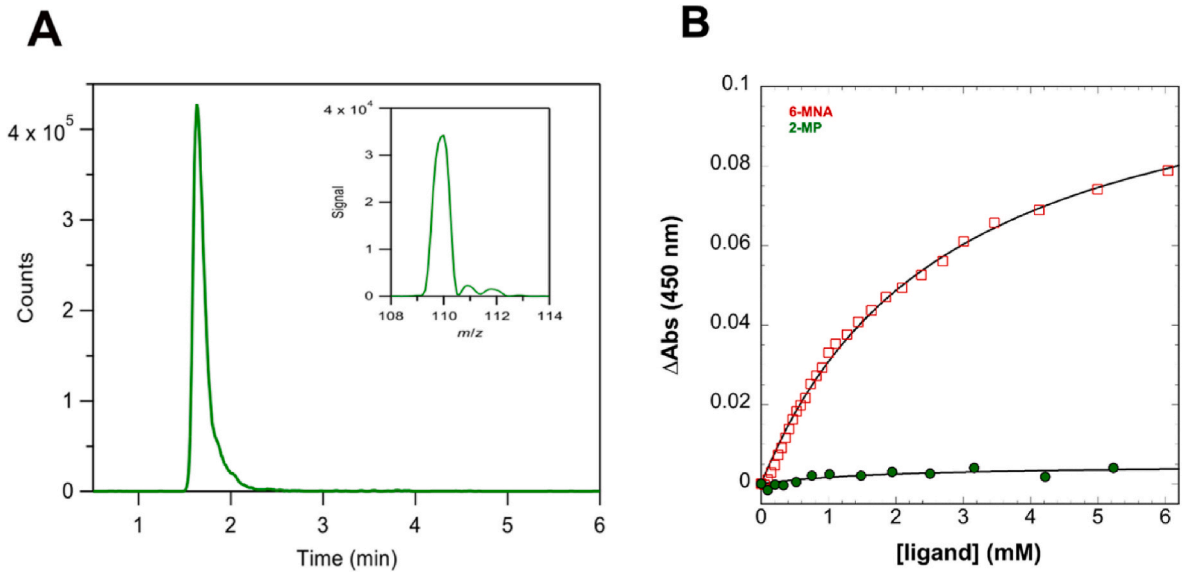

Fig. 2. 2-MP is a contaminant that binds the H47Q NicC variant weakly. **A.** Extracted ion chromatogram at $m/z = 110$ showing 2-MP ($C_5H_4NS^-$) present in the starting material. The inset shows the corresponding mass spectrum at a retention time of 1.63 min. **B.** Equilibrium titrations of the H47Q variant of NicC (30 μM) with 6-MNA (red squares) and 6-MP (green circles) fit to the hyperbolic binding equation estimates a K_d for E·6-MNA of 2.9 ± 0.1 mM and K_d for E·2-MP of 2.0 ± 1.8 mM.

MP in the resulting crystal structure. The structures of 6-MNA and 2-MP, with atom numbering, are shown in Scheme S1.

2-MP is a contaminant that is non-catalytic. Based on our previous kinetic analyses with wild type NicC and 6-HNA as well as several substrate analogues [10,11,20], 2-MP is not an expected intermediate in the NicC-catalyzed reaction. The 6-MNA stock was purchased from a commercial source (Sigma Aldrich) at the highest possible purity, approximately 90%, available. As shown in Fig. 2A, mass spectrometric analysis of the 6-MNA from this commercial stock indicates that 2-MP is present as an impurity. Thus, the 2-MP present in the NicC active site likely originated as a contaminant from the 6-MNA stock, rather than as a reaction intermediate.

As shown in Fig. 2B, equilibrium binding studies indicate that 2-MP binds very weakly, and elicits only a small perturbation in the absorbance at 450 nm, to H47Q NicC with an estimated lower limit for K_d of 2.0 ± 1.8 mM. As the error on this measurement is very high, the K_d for the E•2-MP complex could be as high as ~4 mM. For comparison, the K_d for E•6-MNA (Fig. 2B) is 2.8 ± 0.1 mM indicating that both 6-MNA and 2-MP bind H47Q *P. putida* NicC very weakly. Together these data indicate that a hydroxyl at position 6 plays an important role in substrate affinity. These low binding affinities help explain the weak electron density observed for the ligand in the active site. In comparison, the K_d for the wild type NicC•6-HNA is 58 ± 12 μM [11], a greater than 34-fold binding enhancement stemming from the 6-OH *vs.* 6-SH substituent. Likewise, kinetic analysis of turnover with 2-MP indicates that this molecule is not a substrate for wild type or H47Q NicC (Fig. S7) as there is no evidence that 2-MP is transformed by either enzyme or converted to the expected 2-M-5-P product. Instead, kinetic analysis indicates that 2-MP is a non-catalytic molecule that was fortuitously trapped in the H47Q NicC active site.

Details of the 2-MP binding site. The 2-MP binding site is shown in Fig. 3A. This binding site contains many aromatic residues including Trp273 which π stacks to the 2-MP ligand. There are also two tyrosine residues (Tyr215 and Try225) near the 2-MP thiol. The glutamine residue at position 47, which is naturally a histidine, is located near Tyr215 (4.9 Å to the closest side chain atom). This model for substrate binding concurs with our understanding of how 6-HNA binds, based on the data reported earlier for the *B. bronchiseptica* H47E and Y215F variants [11]. A histidine residue at position 211, previously thought to be involved in ligand binding [10], is not near the 2-MP binding pocket.

In this structure, the 2-MP is located near the FAD isoalloxazine ring, which is in the "in" conformation. The C5 atom of 2-MP, the site of hydroxylation for the natural substrate, is 7.6 Å from the C4a of the FAD isoalloxazine ring which approximately 2 Å further than what has been seen in the crystal structures of comparable Class A flavin monooxygenases. The C4a atom is the site of hydroxyl transfer from the hydroperoxide FAD intermediate to the substrate. For comparison, in HpxO the distance between C4a atom of FAD and the site of hydroxylation is 4.9 Å [24]. This distance is 5.5 Å in 2-methyl-3-hydroxypyridine-5-carboxylic acid oxygenase (MHPCO) [25]. In the 2-MP bound structure, the thiol on 2-MP is within hydrogen bonding distance to Tyr225 (2.9 Å) although the angle is almost perpendicular making it unlikely that the two residues could form a hydrogen bond. As shown in Figure 3A, the thiol is located 4.2 Å from the closest atom in Tyr215. The hydroxyl of Tyr215 and the 2-MP thiol are in a linear arrangement with a bond angle of ~176° making it more likely that these two atoms could form a hydrogen bond if the ligand and/or residue side chain moved slightly (approximately 1–1.5 Å). Therefore, it is likely that there is a conformational change prior to catalysis that allows Tyr215 to abstract a proton from the substrate, as has been previously postulated based on kinetic analysis [11].

Interestingly, Arg184 is well positioned to play an important role in substrate binding. In Fig. 3B, the unliganded H47Q NicC structure is superimposed on the H47Q NicC•2-MP structure. In the unliganded H47Q NicC structure, the side chain of Arg184 binds in the same position as 2-MP. Specifically, Arg184 binds near where carbon 3 of the native 6-HNA substrate would bind; carbon 3 contains the carboxylate group on the native substrate (Scheme 1 and Scheme S1). Arg184 becomes completely disordered upon substrate binding and its side chain could not be modeled in to the liganded structure. As shown by primary sequence alignment (Fig. S8), Arg184 is somewhat conserved in Class A flavin monooxygenases as it is present also in salicylate hydroxylase (PDB ID: 6BZ5, 31% identical to NicC) [26] and 3-hydroxybenzoate

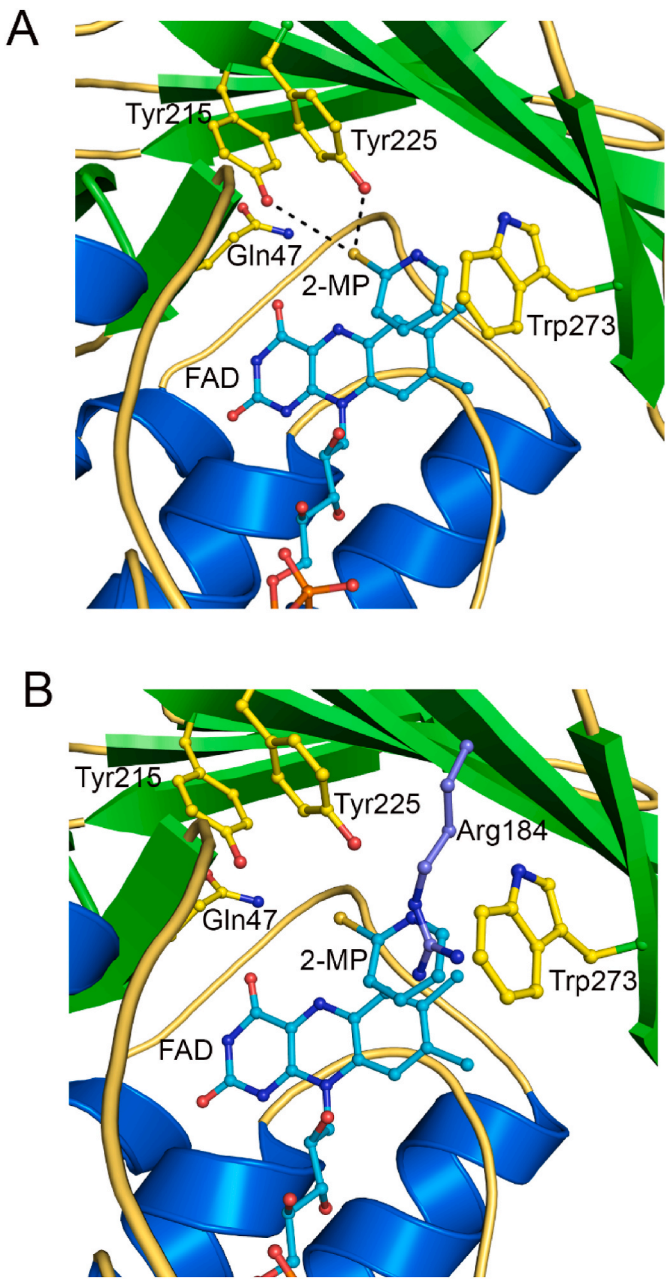

Fig. 3. The H47Q NicC active site. **A.** Residues in the 2-MP binding pocket are highlighted. H47Q NicC protein residues are shown in ball and stick mode with yellow carbon atoms, red oxygen atoms, blue nitrogen atoms, orange phosphorous atoms, and dark yellow sulfur atoms. The protein is colored by secondary structure with α-helicies in blue, β-strands in green, and loops in yellow. FAD and 2-MP are also shown in ball and stick mode with cyan carbon atoms. Potential interactions are highlighted with dashed black lines. **B.** The potential role of Arg184 in substrate binding is highlighted. An overlay of the H47Q NicC structures in the presence and absence of 2-MP is shown. Coloring as in Part A. In addition, Arg184 from the unliganded H47Q NicC structure is shown with purple carbon atoms and dark purple nitrogen atoms. The side chain of Arg184 is disordered in the liganded H47Q NicC structure.

6-hydroxylase (PDB ID: 4BK2, 32% identical to NicC) [27]. Changes in the conformation of an arginine side chain upon ligand binding has been seen in other flavin dependent monooxygenases demonstrating that Arg184 may be involved in stabilizing ligand binding through ionic interactions [28,29]. These structural studies reveal that an arginine may play a critical role in substrate binding and catalysis for the NicC-catalyzed reaction.

As shown in Fig. 4, NicC has a conserved water network that is present both in the wild type enzyme (Fig. 4A) and the unliganded, H47Q variant (Fig. 4B). These water molecules mark the position of the ligand binding site (Fig. 3A). The archetypical Class A flavin monooxygenase, *p*-hydroxybenzoate hydroxylase, also has a network of water

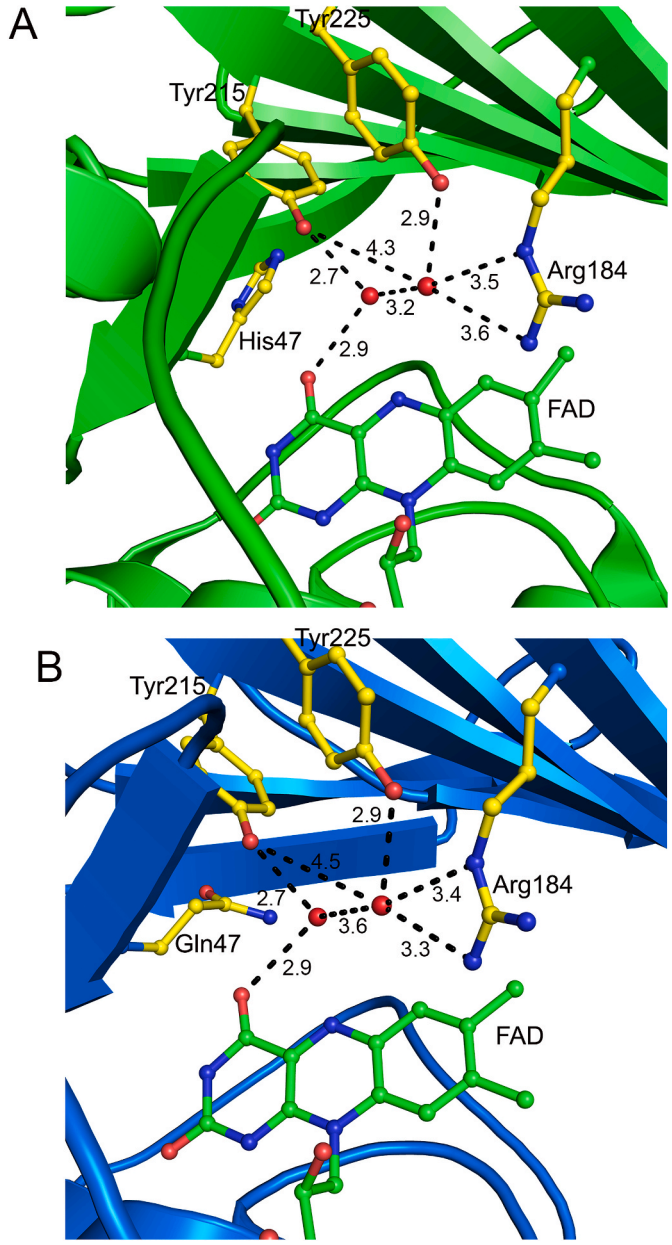

Fig. 4. The conserved water network in NicC. **A.** The wild type NicC has two water molecules that mark the 2-MP binding site in the liganded H47Q NicC structure. Carbon atoms are shown in yellow for the NicC residues and in green for the FAD coenzyme, oxygen atoms are shown red, and nitrogen atoms in blue. The ribbon structure is shown in green. Distances are shown in Angstroms (Å) with dashed black lines. **B.** The same water molecules are also conserved in the H47Q NicC structure. The ribbon structure is shown in blue, the rest of the coloring is the same as in Part A.

molecules that link active site residues to the substrate [30,31]. In both unliganded NicC structures (wild type and H47Q), one of the water molecules is positioned 2.7 Å away from Tyr215, the putative general base [11]. This water is therefore well-positioned to become deprotonated by Tyr215 and act as a base. A similar strategy has been suggested for the mechanism of PHBH [30]. However, in the liganded structure, this water molecule is not present. This is perhaps because we have captured a catalytically inactive E•2-MP complex. This possibility is discussed in further detail below.

Mechanistic Implications. NicC catalyzes the decarboxylative hydroxylation of 6-HNA to 2,5-dihydroxypyridine with near stoichiometric oxidation of NADH to NAD^+ [11]. Although the 2-MP electron density is weak, it is in the same location as the previously uninterpretable electron density, mentioned previously, and there is also clear sulfur difference density in the active site (Fig. S6) indicative of bound 2-MP. Thus, the H47Q NicC•2-MP structure provides information about the molecular level details of the NicC-catalyzed reaction. In addition, these structural data are mainly consistent with the mechanism previously proposed [11]. For example, here we do not observe that the hydroxyl group putative active site base, Tyr215, and the thiol on the substrate analogue are within hydrogen bonding distance as we would predict from the kinetic analysis. We also do not observe a bridging water molecule that could link Tyr215 and 2-MP via a water-mediated hydrogen bond. When Tyr215 was mutated to phenylalanine, the resulting variant had a product coupling ratio of 0.0048 indicating that this residue is critical for substrate hydroxylation as the product coupling ratio is a measure of the relative extent of formation of hydroxylated product to NAD^+.. The Y215F variant also had a 240-fold weaker binding affinity for 6-HNA and a relative rate constant for substrate hydroxylation that was 0.05% that of the wild-type enzyme (Table S3) [11].

The structural model shows that Tyr215 and 2-MP are in a linear arrangement indicating that there might be a conformational change that occurs prior to catalysis allowing Tyr215 to deprotonate the hydroxyl on carbon 6 of the substrate leading to product formation (Fig. S9A). It is possible that the conserved water molecule observed in the wild-type and unliganded variant structures (Fig. 4) is also present in the catalytically relevant enzyme conformation and deprotonates the substrate (Fig. S9B). Thus, due to the absence of a direct or water-mediated interaction between the enzyme residues and the 2-MP ligand, it is likely that we have trapped a catalytically inactive enzymatic state consistent with our data that demonstrate that 2-MP is not a NicC substrate. However, due to the position of the 2-MP thiol group near both Tyr215 and the predicted location of His47, the 2-MP orientation could be similar to the catalytic orientation of the 6-HNA substrate in the active E•S complex as both Tyr215 and His47 have previously been shown to be critical for catalysis [11].

4. Conclusions

Although flavin monooxygenases have been well-examined in the biochemical literature [12,32], scientists are still discovering new aspects of their catalysis including recent work that has shown that these enzymes can be involved in redox chemistry and covalent catalysis [33]. The ligand bound structure of the H47Q NicC variant has revealed that Trp273 and Arg184 may play an important role in substrate binding and will be the focus of future kinetic and thermodynamic studies. Recent preliminary data also indicate that the E•S complex is more flexible in solution than the free enzyme, which could help explain our previous difficulties in obtaining a ligand-bound structure of NicC. This liganded H47Q NicC structure is significant in illuminating how NicC catalyzes its unique decarboxylative hydroxylation reaction.

Funding

This work was funded by the National Science Foundation (MCB

1817535 to M.J.S. and 1817633 to K.A.H.).

CRediT authorship contribution statement

Zachary R. Turlington: Investigation, Writing – original draft. **Sofia Vaz Ferreira de Macedo:** Investigation. **Kay Perry:** Data curation, Formal analysis. **Sam L. Belsky:** Investigation. **Jennifer A. Faust:** Formal analysis, Investigation. **Mark J. Snider:** Conceptualization, Data curation, Formal analysis, Funding acquisition, Investigation, Methodology, Resources, Supervision, Writing – original draft, Writing – review & editing. **Katherine A. Hicks:** Conceptualization, Data curation, Formal analysis, Funding acquisition, Investigation, Methodology, Project administration, Resources, Software, Supervision, Validation, Visualization, Writing – original draft, Writing – review & editing.

Acknowledgements

We thank Andrew Roering and Francis Rossi, both at SUNY Cortland, for helpful discussion about this work. Ryan Campbell from the College of Wooster is acknowledged for collecting the spectrum of 6-mercaptopyridine-3-carboxylic acid (6-MNA) that is included in the Supplemental Information.

This work is based upon research conducted at the Northeastern Collaborative Access Team beamlines, which are funded by the National Institute of General Medical Sciences from the National Institutes of Health (P30 GM124165). The Eiger 16 M detector on 24-ID-E is funded by a NIH-ORIP HEI grant (S10OD021527). This research used resources of the Advanced Photon Source, a U.S. Department of Energy (DOE) Office of Science User Facility operated for the DOE Office of Science by Argonne National Laboratory under Contract No. DE-AC02-06CH11357.

Appendix A. Supplementary data

Supplementary data to this article can be found online at https://doi.org/10.1016/j.abb.2023.109859.

References

[1] K.K. Barnes, D.W. Kolpin, E.T. Furlong, S.D. Zaugg, M.T. Meyer, L.B. Barber, A national reconnaissance of pharmaceuticals and other organic wastewater contaminants in the United States–I) groundwater, Sci. Total Environ. 402 (2–3) (2008) 192–200, https://doi.org/10.1016/j.scitotenv.2008.04.028.

[2] E. Bokor, J. Amon, M. Varga, A. Szekeres, Z. Hegedus, T. Jakusch, Z. Szakonyi, M. Flipphi, C. Vagvolgyi, A. Gacser, et al., A complete nicotinate degradation pathway in the microbial eukaryote Aspergillus nidulans, Commun. Biol. 5 (1) (2022) 723, https://doi.org/10.1038/s42003-022-03684-3.

[3] Y. Guo, D.F. Li, H. Ji, J. Zheng, N.Y. Zhou, Hexachlorobenzene monooxygenase substrate selectivity and catalysis: structural and biochemical insights, Appl. Environ. Microbiol. 87 (1) (2020), https://doi.org/10.1128/AEM.01965-20. From NLM Medline. Bi, E.; Schmidt, T. C.; Haderlein, S. B. Environmental factors influencing sorption of heterocyclic aromatic compounds to soil. Environ Sci Technol 2007, 41 (9), 3172-3178. DOI: 10.1021/es0623764.

[4] K. Hirao, Y. Shinohara, H. Tsuda, S. Fukushima, M. Takahashi, Carcinogenic activity of quinoline on rat liver, Cancer Res. 36 (2 Pt 1) (1976) 329.

[5] M.J. Focazio, D.W. Kolpin, K.K. Barnes, E.T. Furlong, M.T. Meyer, S.D. Zaugg, L. B. Barber, M.E. Thurman, A national reconnaissance for pharmaceuticals and other organic wastewater contaminants in the United States–II) untreated drinking water sources, Sci. Total Environ. 402 (2–3) (2008) 201–216, https://doi.org/10.1016/j.scitotenv.2008.02.021.

[6] L. Lian, S. Yan, B. Yao, S.A. Chan, W. Song, Photochemical transformation of nicotine in wastewater effluent, Environ. Sci. Technol. 51 (20) (2017) 11718–11730, https://doi.org/10.1021/acs.est.7b03223.

[7] G.K. Sims, E.J. O'Loughlin, Degradation of pyridines in the environment, Crit. Rev. Environ. Control 19 (4) (1989) 309–340.

[8] V. Pakova, K. Hilscherova, M. Feldmannova, L. Blaha, Toxic effects and oxidative stress in higher plants exposed to polycyclic aromatic hydrocarbons and their N-heterocyclic derivatives, Environ. Toxicol. Chem. 25 (12) (2006) 3238–3245, https://doi.org/10.1897/06-162r.1.

[9] J.I. Jimenez, A. Canales, J. Jimenez-Barbero, K. Ginalski, L. Rychlewski, J. L. Garcia, E. Diaz, Deciphering the genetic determinants for aerobic nicotinic acid degradation: the nic cluster from Pseudomonas putida KT2440, Proc. Natl. Acad. Sci. U.S.A. 105 (32) (2008) 11329–11334, https://doi.org/10.1073/pnas.0802273105.

[10] K.A. Hicks, M.E. Yuen, W.F. Zhen, T.J. Gerwig, R.W. Story, M.C. Kopp, M.J. Snider, Structural and biochemical characterization of 6-hydroxynicotinic acid 3-monooxygenase, A novel decarboxylative hydroxylase involved in aerobic nicotinate degradation, Biochemistry 55 (24) (2016) 3432–3446, https://doi.org/10.1021/acs.biochem.6b00105.

[11] K.D. Nakamoto, S.W. Perkins, R.G. Campbell, M.R. Bauerle, T.J. Gerwig, S. Gerislioglu, C. Wesdemiotis, M.A. Anderson, K.A. Hicks, M.J. Snider, Mechanism of 6-hydroxynicotinate 3-monooxygenase, a flavin-dependent decarboxylative hydroxylase involved in bacterial nicotinic acid degradation, Biochemistry 58 (13) (2019) 1751–1763, https://doi.org/10.1021/acs.biochem.8b00969.

[12] C.E. Paul, D. Eggerichs, A.H. Westphal, D. Tischler, W.J.H. van Berkel, Flavoprotein monooxygenases: versatile biocatalysts, Biotechnol. Adv. 51 (2021), 107712, https://doi.org/10.1016/j.biotechadv.2021.107712.

[13] P. Chenprakhon, T. Wongnate, P. Chaiyen, Monooxygenation of aromatic compounds by flavin-dependent monooxygenases, Protein Sci. 28 (1) (2019) 8–29, https://doi.org/10.1002/pro.3525.

[14] Z. Dauter, Sulfur-SAD phasing from microcrystals utilizing low-energy X-rays, IUCrJ 6 (Pt 4) (2019) 503–504, https://doi.org/10.1107/S2052252519008698.

[15] S. Iwata, M. Saynovits, T.A. Link, H. Michel, Structure of a water soluble fragment of the 'Rieske' iron-sulfur protein of the bovine heart mitochondrial cytochrome bc1 complex determined by MAD phasing at 1.5 A resolution, Structure 4 (5) (1996) 567–579, https://doi.org/10.1016/s0969-2126(96)00062-7.

[16] J. Agirre, M. Atanasova, H. Bagdonas, C.B. Ballard, A. Basle, J. Beilsten-Edmands, R.J. Borges, D.G. Brown, J.J. Burgos-Marmol, J.M. Berrisford, et al., The CCP4 suite: integrative software for macromolecular crystallography, Acta Crystallogr D Struct Biol 79 (Pt 6) (2023) 449–461, https://doi.org/10.1107/S2059798323003595.

[17] D. Liebschner, P.V. Afonine, M.L. Baker, G. Bunkoczi, V.B. Chen, T.I. Croll, B. Hintze, L.W. Hung, S. Jain, A.J. McCoy, et al., Macromolecular structure determination using X-rays, neutrons and electrons: recent developments in Phenix, Acta Crystallogr D Struct Biol 75 (Pt 10) (2019) 861–877, https://doi.org/10.1107/S2059798319011471.

[18] A. Casanal, B. Lohkamp, P. Emsley, Current developments in coot for macromolecular model building of electron cryo-microscopy and crystallographic data, Protein Sci. 29 (4) (2020) 1069–1078, https://doi.org/10.1002/pro.3791.

[19] C.J. Williams, J.J. Headd, N.W. Moriarty, M.G. Prisant, L.L. Videau, L.N. Deis, V. Verma, D.A. Keedy, B.J. Hintze, V.B. Chen, et al., MolProbity: more and better reference data for improved all-atom structure validation, Protein Sci. 27 (1) (2018) 293–315, https://doi.org/10.1002/pro.3330.

[20] S.W. Perkins, M.Z. Hlaing, K.A. Hicks, L.J. Rajakovich, M.J. Snider, Mechanism of the multistep catalytic cycle of 6-hydroxynicotinate 3-monooxygenase revealed by global kinetic analysis, Biochemistry 62 (10) (2023) 1553–1567, https://doi.org/10.1021/acs.biochem.2c00514.

[21] H.A. Schreuder, A. Mattevi, G. Obmolova, K.H. Kalk, W.G. Hol, F.J. van der Bolt, W.J. van Berkel, Crystal structures of wild-type p-hydroxybenzoate hydroxylase complexed with 4-aminobenzoate,2,4-dihydroxybenzoate, and 2-hydroxy-4-aminobenzoate and of the Tyr222Ala mutant complexed with 2-hydroxy-4-aminobenzoate. Evidence for a proton channel and a new binding mode of the flavin ring, Biochemistry 33 (33) (1994) 10161–10170, https://doi.org/10.1021/bi00199a044.

[22] H.A. Schreuder, P.A. Prick, R.K. Wierenga, G. Vriend, K.S. Wilson, W.G. Hol, J. Drenth, Crystal structure of the p-hydroxybenzoate hydroxylase-substrate complex refined at 1.9 A resolution. Analysis of the enzyme-substrate and enzyme-product complexes, J. Mol. Biol. 208 (4) (1989) 679–696, https://doi.org/10.1016/0022-2836(89)90158-7.

[23] J. Wang, M. Ortiz-Maldonado, B. Entsch, V. Massey, D. Ballou, D.L. Gatti, Protein and ligand dynamics in 4-hydroxybenzoate hydroxylase, Proc. Natl. Acad. Sci. U.S.A. 99 (2) (2002) 608–613, https://doi.org/10.1073/pnas.022640199.

[24] K.A. Hicks, S.E. O'Leary, T.P. Begley, S.E. Ealick, Structural and mechanistic studies of HpxO, a novel flavin adenine dinucleotide-dependent urate oxidase from Klebsiella pneumoniae, Biochemistry 52 (3) (2013) 477–487, https://doi.org/10.1021/bi301262p.

[25] K.M. McCulloch, T. Mukherjee, T.P. Begley, S.E. Ealick, Structure of the PLP degradative enzyme 2-methyl-3-hydroxypyridine-5-carboxylic acid oxygenase from Mesorhizobium loti MAFF303099 and its mechanistic implications, Biochemistry 48 (19) (2009) 4139–4149, https://doi.org/10.1021/bi900149f.

[26] D.M.A. Costa, S.V. Gomez, S.S. de Araujo, M.S. Pereira, R.B. Alves, D.C. Favaro, A. C. Hengge, R.A.P. Nagem, T.A.S. Brandao, Catalytic mechanism for the conversion of salicylate into catechol by the flavin-dependent monooxygenase salicylate hydroxylase, Int. J. Biol. Macromol. 129 (2019) 588–600, https://doi.org/10.1016/j.ijbiomac.2019.01.135.

[27] S. Montersino, R. Orru, A. Barendregt, A.H. Westphal, E. van Duijn, A. Mattevi, W. J.H. van Berkel, Crystal structure of 3-hydroxybenzoate 6-hydroxylase uncovers lipid-assisted flavoprotein strategy for regioselective aromatic hydroxylation, J. Biol. Chem. 288 (36) (2013) 26235–26245, https://doi.org/10.1074/jbc.M113.479303.

[28] P.J. Goldman, K.S. Ryan, M.J. Hamill, A.R. Howard-Jones, C.T. Walsh, S.J. Elliott, C.L. Drennan, An unusual role for a mobile flavin in StaC-like indolocarbazole biosynthetic enzymes, Chem. Biol. 19 (7) (2012) 855–865, https://doi.org/10.1016/j.chembiol.2012.05.016.

[29] M.S. Manenda, M.E. Picard, L. Zhang, N. Cyr, X. Zhu, J. Barma, J.M. Pascal, M. Couture, C. Zhang, R. Shi, Structural analyses of the Group A flavin-dependent monooxygenase PieE reveal a sliding FAD cofactor conformation bridging OUT and IN conformations, J. Biol. Chem. 295 (14) (2020) 4709–4722, https://doi.org/10.1074/jbc.RA119.011212.

[30] D.L. Gatti, B. Entsch, D.P. Ballou, M.L. Ludwig, pH-dependent structural changes in the active site of p-hydroxybenzoate hydroxylase point to the importance of proton and water movements during catalysis, Biochemistry 35 (2) (1996) 567–578, https://doi.org/10.1021/bi951344i.
[31] J. Clarkson, B.A. Palfey, P.R. Carey, Probing the chemistries of the substrate and flavin ring system of p-hydroxybenzoate hydroxylase by Raman difference spectroscopy, Biochemistry 36 (41) (1997) 12560–12566, https://doi.org/10.1021/bi9715270.
[32] A. Phintha, P. Chaiyen, Unifying and versatile features of flavin-dependent monooxygenases: diverse catalysis by a common C4a-(hydro)peroxyflavin, J. Biol. Chem. 299 (12) (2023), 105413, https://doi.org/10.1016/j.jbc.2023.105413.
[33] V. Piano, B.A. Palfey, A. Mattevi, Flavins as covalent catalysts: new mechanisms emerge, Trends Biochem. Sci. 42 (6) (2017) 457–469, https://doi.org/10.1016/j.tibs.2017.02.005.